Nitrous oxide dimer: An *ab initio* coupled-cluster study of isomers, interconversions, and infrared fundamental bands, and experimental observation of a new fundamental for the polar isomer

G. M. Berner,[1] A. L. L. East,[1,a] Mahin Afshari,[2] M. Dehghany,[2] N. Moazzen-Ahmadi,[2,b] and A. R. W. McKellar[3]

[1]*Department of Chemistry and Biochemistry, University of Regina, Regina, Saskatchewan S4S 0A2, Canada*
[2]*Department of Physics and Astronomy, University of Calgary, 2500 University Drive North West, Calgary, Alberta T2N 1N4, Canada*
[3]*Steacie Institute for Molecular Sciences, National Research Council of Canada, Ottawa, Ontario K1A 0R6, Canada*

Improved quantum chemistry (coupled-cluster) results are presented for spectroscopic parameters and the potential energy surface for the N_2O dimer. The calculations produce three isomer structures, of which the two lowest energy forms are those observed experimentally: a nonpolar C_{2h}-symmetry planar slipped-antiparallel geometry (with inward-located O atoms) and a higher-energy polar C_s-symmetry planar slipped-parallel geometry. Harmonic vibrational frequencies and infrared intensities for these isomers are calculated. The low-frequency intermolecular vibrational mode predictions should be useful for future spectroscopic searches, and there is good agreement in the one case where an experimental value is available. The frequency shifts for the high-frequency intramolecular stretching vibrations, relative to the monomer, were calculated and used to help locate a new infrared band of the polar isomer, which corresponds to the weaker out-of-phase combination of the ν_1 antisymmetric stretch of the individual monomers. The new band was observed in the region of the monomer ν_1 fundamental for both $(^{14}N_2O)_2$ and $(^{15}N_2O)_2$ using a tunable infrared diode laser to probe a pulsed supersonic jet expansion, and results are presented. © *2009 American Institute of Physics.* [DOI: 10.1063/1.3121224]

I. INTRODUCTION

The primary purpose of this paper is to present improved quantum chemistry results for (i) spectroscopic constants and (ii) the potential energy surface (PES) for conformer interconversion, for the gas-phase N_2O dimer. Previous *ab initio* studies on N_2O dimer of a similar nature, but at lower levels of theory, have been reported by Sadlej and Sicinski,[1] Mogi *et al.*,[2] Nxumalo *et al.*,[3] and by Valdés and Sordo.[4] The spectroscopic constants (vibrational fundamentals and rotational constants) are needed to keep pace with recent experimental observations of the spectra of the N_2O dimer and to point the way to possible future experiments. The PES investigations are needed to investigate why, of the four predicted conformers[3,4] of the dimer, only two have been observed to date.

The experimental data available for the nitrous oxide dimer greatly expanded in the last two years. Previous to this, $(N_2O)_2$ had been observed by means of infrared spectra in the regions of the monomer vibrations $\nu_1 + \nu_3$ (~ 3500 cm^{-1}),[5] $\nu_1(\sim 2220$ cm$^{-1})$,[6] and $\nu_3(\sim 1280$ cm$^{-1})$,[7] all of which showed a nonpolar form of the dimer with a slipped antiparallel geometry having C_{2h} symmetry. In 2007, we discovered a new polar isomer of $(N_2O)_2$ by means of its spectrum in the ν_1 region,[8] and later the ν_3 region.[9] With the

help of these infrared results, the polar dimer has now been observed in the microwave region by means of its pure rotational spectrum.[10] It turns out to have a planar slipped parallel structure with C_s symmetry. As well, the nonpolar N_2O dimer studies have been extended to the fully substituted ^{15}N isotopomer[11] and the earlier assignment of a combination band (~ 2249 cm^{-1}) involving the intermolecular torsional vibration has been corrected.[12]

In the nonpolar dimer, the two monomers are equivalent, so vibrational modes corresponding to in-phase monomer stretching vibrations are infrared inactive. Each monomer stretch is therefore accompanied by only one infrared active dimer mode, corresponding to the out-of-phase combination. In the case of the polar dimer, the two monomers are no longer equivalent and so two allowed dimer modes should accompany each monomer stretch. However, only one of these bands was previously detected in each monomer stretching region. With the help of the present *ab initio* results, we have now been able to locate the other polar dimer band in the monomer ν_1 region; hence the secondary purpose of this paper is to report this new experimentally measured spectrum.

We suspected that the nonexistence of two of the four predicted isomers of this dimer might be due to low interconversion barriers via a particularly labile disrotatory (gearing-motion) cycle. Such a cycle is known for benzene dimer, where it connects T-shaped and slipped-parallel

a)Electronic mail: allan.east@uregina.ca.
b)Electronic mail: ahmadi@phas.ucalgary.ca.

TABLE I. Computed relative energies (cm^{-1}) of optimized isomers of $(N_2O)_2$.

Level of theory	Nonpolar (O-in)	Polar	T-shape N-in	Nonpolar N-in	End to End	D_e (Nonpolar O-in)
			Present results			
PW91/aug-cc-pVTZ	0	30	9	50	244	325
MP2/aug-cc-pVDZ	0	−37	38	7	451	690
MP2/aug-cc-pVDZ[a]	0	−23	32	100	452	653
MP3/aug-cc-pVDZ[a]	0	272	283	465	618	702
MP3/aug-cc-pVTZ[a]	0	260	295	444	648	704
CCSD/aug-cc-pVDZ[a]	0	246	263	422	557	710
CCSD/aug-cc-pVTZ[a]	0	237	275	408	588	707
CCSD(T)/aug-cc-pVDZ[a]	0	185	187	338	539	747
CCSD(T)/aug-cc-pVTZ[a]	0	176	231	325	577	761
			Previous results			
MP2/6–31G(d)[b]	0	−22	28	55		629
MP2/aug-cc-pVDZ[c]	0	−31	34	14		581[d]
MP2/cc-pVTZ[c]	0	−33	12	10		449[d]
MP4/aug-cc-pVDZ[c]	0	−73	27	−1		546[d]
QCISD(T)/aug-cc-pVDZ[c]	0	180	199	358		604[d]

[a]Calculated using CCSD/aug-cc-pVDZ geometries.
[b]Reference 3.
[c]Reference 4, calculated using MP2/cc-pVTZ geometries, and includes zero-point vibrational energies.
[d]D_o values, add ~100 cm^{-1} for D_e.

structures,[13] and acetylene dimer, where it interconverts T-shaped structures.[14] For $(N_2O)_2$, two isomers have been detected by gas-phase spectroscopy, one polar and one nonpolar, and both with planar slipped-parallel structures. We will demonstrate below that three potential minima are predicted by coupled-cluster calculations, that a disrotatory cycle connects all three, and that the barrier separating the T-shaped structure from the polar one is quite small, possibly preventing the T-shaped structure from being uniquely observable experimentally.

II. COMPUTATIONAL RESULTS

A. Computational methods

All calculations were performed with GAUSSIAN03,[15] using several theoretical methods: a density-functional approximation (PW91),[16] Møller–Plesset perturbation theory to second and third order (MP2, MP3),[17] and coupled-cluster approximations [CCSD, CCSD(T)].[18–20] The MP and CC calculations were frozen core. Dunning augmented basis sets[21,22] were used. Energy-minimized conformers and transition states were both fully optimized with three levels of theory: PW91/aug-cc-pVTZ, MP2/aug-cc-pVDZ, and CCSD/aug-cc-pVDZ. Additional relative energies were obtained with single-point calculations based on CCSD/aug-cc-pVDZ optimized geometries. Counterpoise calculations for basis-set superposition error were computed for unrelaxed monomers, using the automated command in GAUSSIAN03.

B. Energies and the potential energy surface

Structures of several conformers known from past studies were investigated and a summary of raw relative energies (without zero-point or basis-set superposition corrections) appears in Table I. The best results should be those at the CCSD, CCSD(T), and QCISD(T) levels. The aug-cc-pVDZ basis set very well reproduces the results with the more expensive aug-cc-pVTZ basis set and CCSD results are within 100 cm^{-1} of CCSD(T) results, which lends support to our use of CCSD/aug-cc-pVDZ for geometry optimization and vibrational frequency calculations.

Note that MP2 and PW91 are not expected to be accurate within 1 kcal/mol (350 cm^{-1}), so the relative energy problems of these methods on this scale should not be surprising. The artificial lowering of the nonpolar N-in dimer at these lower levels of theory might be attributed to overweighting of the secondary Lewis structure for NNO that involves two double bonds and partial negative charge on the outer nitrogen, since this would give additional electrostatic benefits to this structure, as well as giving shifts in the relative NN versus NO bond lengths that are seen (data not shown). However, the trends with the T-shaped structure suggest interesting quadrupole effects as well.

To date, only the first two isomers in Table I have been observed spectroscopically: the slipped-antiparallel nonpolar O-in and the slipped-parallel polar forms. Since the best *ab initio* calculations predict the T-shaped N-in isomer to be quite close in energy to the known polar isomer, transition state calculations were performed to determine barrier heights for both in-plane and out-of-plane interconversions.

In-plane interconversion occurs via the disrotatory cycle (Fig. 1), which connects four of the five structures of Table I, including the two spectroscopically detected isomers at $x = 0°$ and $\sim 90°$, where x is the disrotatory angle as defined in Fig. 2. The transition states were computed at three levels of theory (see Sec. II A), hereafter referred to by their methods only: PW91, MP2, and CCSD. These results are shown as sketches of PES energy profiles in Fig. 3. Note that two of the points in this plot may not really be stationary points: the PW91 structures at $x = 90°$ (polar) and $x = 95°$ (transition state from polar to T-shape N-in) each produced a vibrational fre-
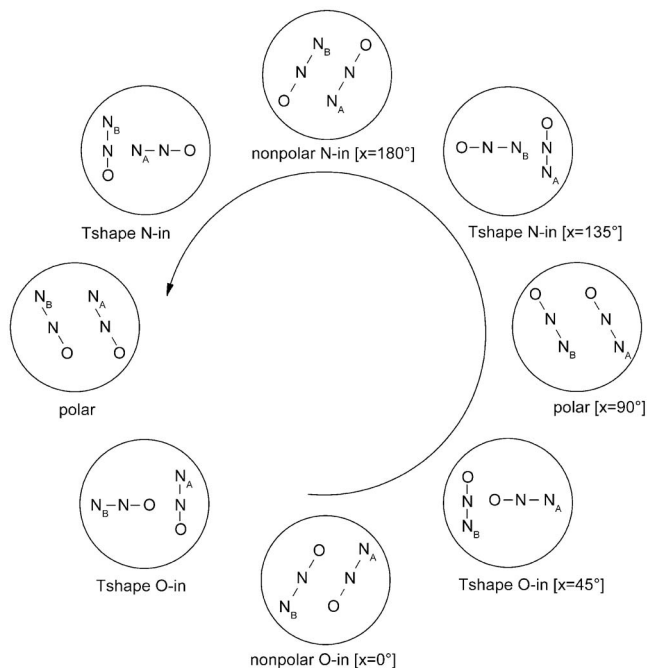
FIG. 1. Illustration of the disrotatory cycle. As one moves counterclockwise in the cycle, monomer *A* moves clockwise while monomer *B* moves counterclockwise. Values for the disrotatory coordinate *x* (defined in Fig. 2) are shown; note that the left half of the cycle is indistinguishable from the right half except for atom identities.

quency that was indistinguishable from the noise of the rotational frequency zeros (<8 cm^{-1}). From Fig. 3, the first remark is that MP2 and PW91 appear to have problems throughout the cycle. Focusing on the CCSD PES only, the second remark is that the T-shaped N-in structure is separated from the polar slipped-parallel structure by a very small barrier (11 cm^{-1}, or 0.1 kJ/mol), which suggests two reasons why the T-shaped isomer may not be observable: (i) this barrier may not exist on the true PES or (ii) the zero-point or thermal energy of the dimer in the supersonic jet are sufficient to allow interconversion of these two forms. In either scenario, the implication is that the polar isomer has a very low frequency (large-amplitude) vibrational mode for disrotation.

We also searched for out-of-plane pathways between minimum-energy structures, as shown in Fig. 4. On the MP2
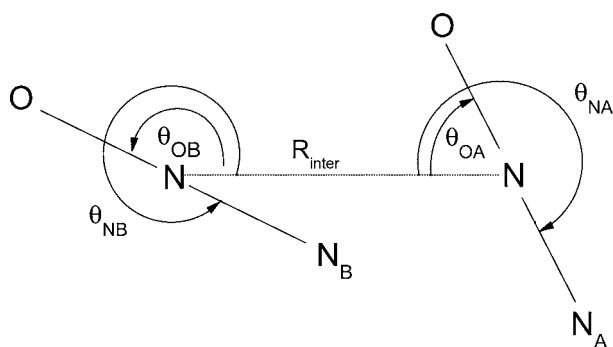

FIG. 2. Definition of the disrotatory coordinate *x*: the average of the two directional angles θ_{OA} and θ_{OB}. *x* ranges from -180 to $+180$ if θ_{OB} is defined from -120 to $+240$, and θ_{OA} from -240 to $+120$, with positive directions as defined by the arrows.
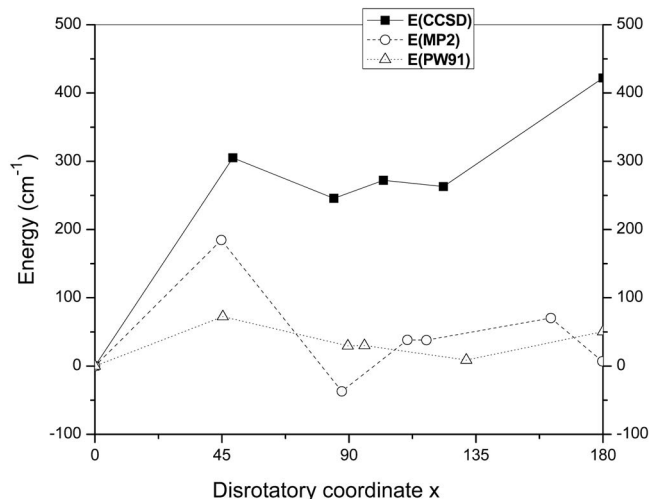

FIG. 3. PES for disrotatory cycle of N$_2$O dimer, computed at three levels of approximation. The CCSD approximation is expected to be the most accurate and it correctly predicts the $x=0°$ "nonpolar O-in" structure to be the most abundant.

PES, there is a high-energy cross-structure intermediate, through which all slipped-parallel structures can interconvert. On the PW91 PES, the cross-structure intermediate disappears, but there is still a skewed-cross out-of-plane transition state for polar/nonpolar isomerization. However, on the more accurate CCSD PES, both the minimization and the transition-state search went to planar structures, indicating no out-of-plane stationary points for isomerization. We conclude that out-of-plane isomerization mechanisms are not important for this dimer.

C. *Ab initio* geometries and rotational constants

The optimized CCSD geometries are given in Table II. To demonstrate their comparative reliability, Table III compares the resulting CCSD rotational constants with the lower levels of theory (MP2 and PW91) and with experiment for the two isomers that have been experimentally observed (nonpolar "O-in" and polar). The CCSD results are indeed the best, producing rotational constants within 3% of experi-
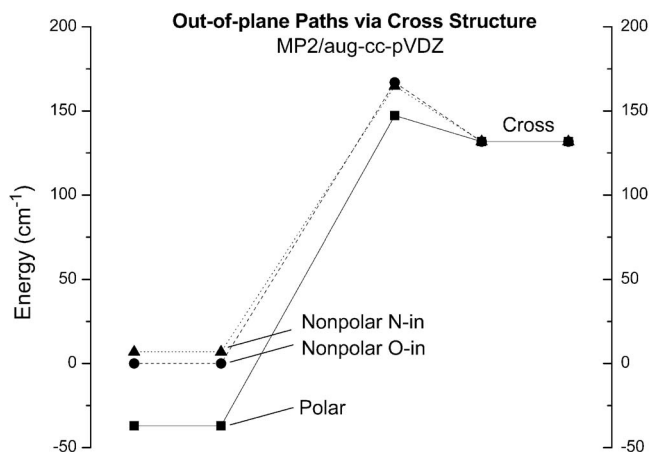

FIG. 4. Schematic for the computed MP2/aug-cc-pVDZ transition-state pathways via cross structure. Out-of-plane pathways through stationary points do not exist on the more accurate CCSD/aug-cc-pVDZ PES.

TABLE II. CCSD/aug-cc-pVDZ geometrical parameters of N_2O dimers.

Coordinate[a]	Nonpolar O-in	Polar	T-shape N-in
R_{NNA}(Å)	1.1353	1.1359	1.1360
R_{NNB}(Å)	1.1353	1.1369	1.1364
R_{NOA}(Å)	1.1995	1.1991	1.1976
R_{NOB}(Å)	1.1995	1.1950	1.1960
R_{inter}(Å)	3.43	3.57	4.14
θ_{OB} (deg)	59.0	114.6	163.2
θ_{NB} (deg)	−121.1	−65.5	−16.8
θ_{OA} (deg)	−59.0	54.8	80.1
θ_{NA} (deg)	121.1	−125.2	−99.9
X (deg)	0.0	84.7	121.6

[a]Coordinates defined in Fig. 2.

mental values. The PW91 results are the worst, producing B and C constants that are too small because the binding energy at this level of theory is too low (D_e, Table I), giving a larger intermolecular distance which increases the moments of inertia and decreases B and C. The MP2 results are good for the nonpolar isomer, but for the polar isomer MP2 produces too strong a binding energy, giving a smaller intermolecular distance, which increases B and C. Table IV lists the most reliable rotational constants (CCSD) for some unobserved isomers and isotopomers as a guide for future research.

D. Dissociation energy, D_e

As a possible means of improving the D_e predictions in Table I, counterpoise corrections for basis-set superposition error were computed: all dimer basis functions are offered to each monomer. The corrections lower the MP2, CCSD, and CCSD(T) estimates of D_e by 217–243 cm^{-1} (aug-cc-pVDZ) and 155–166 cm^{-1} (aug-cc-pVTZ). For our best estimate of

TABLE IV. Computed CCSD/aug-cc-pVDZ rotational constants for unobserved forms of the N_2O dimer (in cm^{-1}).

Isotopomer	Isomer	A	B	C
$(^{14}N^{14}NO)_2$	T-shape N-in	0.3962	0.039 58	0.035 98
$(^{15}N^{15}NO)_2$	T-shape N-in	0.3844	0.038 25	0.034 79
$(^{14}N^{14}NO)(^{15}N^{15}NO)$	Nonpolar O-in	0.2943	0.060 58	0.050 24

D_e, the BSSE-corrected CCSD(T)/aug-cc-pVTZ//CCSD/aug-cc-pVDZ value is 598 cm^{-1}. We presume an accuracy of only ±200 cm^{-1}.

In the preceding section, it was shown that overestimates and underestimates of the binding energy D_e tend to result in overestimates and underestimates, respectively, of the B and C rotational constants. A D_e value of ~600 cm^{-1} demonstrates that the CCSD/aug-cc-pVDZ D_e(710 cm^{-1}) is an overestimate, so that the CCSD/aug-cc-pVDZ B and C constants should also be slight overestimates, in accord with experiment (Table III).

E. *Ab initio* vibrational frequencies

Complete sets of CCSD/aug-cc-pVDZ harmonic frequency results for the main isotopomers of the two known isomers are presented in Table V. These replace the results of previous calculations at lower levels of theory, reported by Sadlej and Sicinski[1] and by Dutton *et al.*[23] for the nonpolar isomer, and by Nxumalo *et al.*[3] for both isomers; the latter results are included in our table for comparison.

The four low-frequency intermolecular librations are of particular interest; the frequencies for the nonpolar isomer agree with the MP2 values of Nxumalo *et al.*,[3] but the frequencies for the polar isomer do not. So far, only one experimental intermolecular frequency has been reported[12] and its

TABLE III. Computed rotational constants for various forms of the N_2O dimer (in cm^{-1}).

	Rotational constant	CCSD[a]	MP2[a]	PW91[b]	Exp[c]	Percent error CCSD	Percent error MP2	Percent error PW91
Nonpolar O-in $(^{14}N^{14}NO)_2$	A	0.2957	0.2911	0.3074	0.299 409	−1.2	−2.8	+2.7
	B	0.061 70	0.062 32	0.051 17	0.059 925	+3.0	+4.0	−14.6
	C	0.051 05	0.051 33	0.043 87	0.049 836	+2.4	+3.0	−12.0
Polar $(^{14}N^{14}NO)_2$	A	0.3015	0.2825	0.3155	0.309 171	−2.5	−8.6	+2.1
	B	0.055 37	0.062 01	0.046 99	0.054 124	+2.3	+14.6	−13.2
	C	0.046 78	0.050 85	0.040 90	0.045 919	+1.9	+10.7	−10.9
Nonpolar O-in $(^{15}N^{15}NO)_2$	A	0.2919			0.294 027	−0.7		
	B	0.058 72			0.056 413	+4.1		
	C	0.048 89			0.047 247	+3.5		
Polar $(^{15}N^{15}NO)_2$	A	0.2906			0.298 119	−2.5		
	B	0.052 94			0.051 806	+2.2		
	C	0.044 78			0.044 004	+1.8		
Polar "light-inside" $(^{14}N^{14}NO)(^{15}N^{15}NO)$	A	0.2928			0.300 583	−2.6		
	B	0.054 66			0.053 362	+2.4		
	C	0.046 06			0.045 274	+1.7		
Polar "heavy-inside" $(^{15}N^{15}NO)(^{14}N^{14}NO)$	A	0.2992			0.306 490	−2.4		
	B	0.053 68			0.052 439	+2.4		
	C	0.045 51			0.044 730	+1.7		

[a]aug-cc-pVDZ basis set.
[b]aug-cc-pVTZ basis set.
[c]Reference 10 for polar data, Ref. 11 for nonpolar data.

TABLE V. Computed CCSD/aug-cc-pVDZ harmonic frequencies and infrared intensities.

Mode description[a]	Sym.	Intensities (km/mol)	Freqs CCSD/aug-cc-pVDZ (cm^{-1})	Freqs MP2/6-31G(d) (cm^{-1}) [b]
Nonpolar isomer				
anti str, anti combo	b_u	676.01	2334	2250
anti str, sym combo	a_g	0.00	2326	2244
sym str, sym combo	a_g	0.00	1302	1294
sym str, anti combo	b_u	187.75	1299	1292
op bend, sym combo	a_u	8.52	591	584
ip bend, sym combo	a_g	0.00	591	579
op bend, anti combo	b_g	0.00	589	583
ip bend, anti combo	b_u	13.39	586	581
ip co-rotation	a_g	0.00	121	113
Dissociation	a_g	0.00	69	56
ip disrotation	b_u	0.94	49	47
op torsion	a_u	0.30	30	26
Polar isomer				
anti str, N-in monomer	a'	617.22	2326	2267
anti str, O-in monomer	a'	108.98	2324	2248
sym str, N-in monomer	a'	85.36	1314	1293
sym str, O-in monomer	a'	82.33	1299	1291
op bend, N-in monomer	a''	4.95	596	588
ip bend, N-in monomer	a'	8.05	594	580
op bend, O-in monomer	a''	3.59	591	582
ip bend, O-in monomer	a'	3.98	590	578
ip co-rotation	a'	0.26	98	50
Dissociation	a'	0.02	44	107
op torsion	a''	0.00	25	28
ip disrotation	a'	0.12	25	44

[a] ip=in-plane, op=out-of-plane, anti str=monomer ν_1, sym str=monomer ν_3; dissociation=van der Waals stretch, ip co-rotation=ip anti-geared bend, ip disrotation=ip geared bend, and op torsion=op bend.
[b] Reference 3.

comparison with theory is discussed below in Sec. IV.

Also of interest are the high-frequency monomer-stretch modes. Values were obtained for infrared frequency shifts of the ν_1 (mostly N–N stretch) and the ν_3 (mostly N–O stretch) vibrations of the N_2O dimers relative to the respective monomer band origins. These values are presented in Tables VI and VII and compared with the experiment below.

III. EXPERIMENTAL RESULTS

The experiments were carried out at the University of Calgary using a tunable infrared diode laser to probe a pulsed supersonic slit jet, with experimental conditions similar to those in the previous N_2O dimer studies.[8,9,11,12] The isotopically enriched sample of $^{15}N^{15}N^{16}O$ was obtained from Iconisotopes with 99% isotopic purity.

As mentioned in the Sec. I, the observed polar N_2O dimer has a planar slipped-parallel structure with C_s point group symmetry, so we expect two infrared active dimer vibrations from this isomer in the region of the monomer ν_1 fundamental band. The present calculations show that these can be approximately characterized as being due to in-phase and out-of-phase vibrations of the two monomer units, with predicted shifts of +2.3 and −0.3 cm^{-1}, respectively, for the normal isotope (see Table VI). The predicted intensity of the in-phase band (which we label as I) is about six times larger

than that of the out-of-phase band (labeled II), which is consistent with this characterization since in the latter case the dipole moments of the two monomers tend to cancel.

Band I has already been observed and analyzed, both for the normal and the fully ^{15}N-substituted isotopomer.[9,11] In the search for band II, we started with the normal isotope and were able to identify a weak band centered just above the monomer band origin, close to the predicted *ab initio* value from Table VI. Although band II is indeed significantly weaker than band I, it could still be observed with a good signal-to-noise ratio. The main experimental difficulty and the reason why band II was not recognized in our earlier searches[8,11] is that it is overlapped by a band of the N_2O trimer. Our success here in identifying band II can be credited to two factors: the availability of the *ab initio* vibrational shift prediction and the fact that the interfering trimer band has now been analyzed.[24] Part of the observed spectrum is shown in Fig. 5, which also contains simulated spectra of band II and of the N_2O trimer. We estimated that the observed intensity of band II was about four to five times weaker than that of band I, in reasonable agreement with the theoretical ratio (Table VI) of 5.7 (or 4.9 for $^{15}N_2O$ dimer).

The analysis of the new N_2O dimer band was made using the PGOPHER computer program,[25] based on a conventional asymmetric rotor Hamiltonian in the *a*-reduced form.

TABLE VI. Computed CCSD/aug-cc-pVDZ frequency shifts ($\Delta\nu = \nu_{\text{dimer}} - \nu_{\text{monomer}}$) and intensities for N_2O dimers in the region of the monomer ν_1 mode.

Isomer	Isotopomer	Dimer mode	Freq (cm^{-1})	Intensity (km/mol)	Shift (cm^{-1})	Obs shift (cm^{-1}) [a]
Nonpolar	($^{14}N_2 O)_2$	Sym combo	2326.4	0	2.6	
Nonpolar	($^{14}N_2 O)_2$	Antisym combo	2333.8	676	10.0	5.726
Nonpolar	($^{15}N_2 O)_2$	Sym combo	2251.0	0	2.3	
Nonpolar	($^{15}N_2 O)_2$	Antisym combo	2258.2	644	9.5	5.442
Nonpolar	($^{14}N_2 O)($^{15}N_2 O)$	Light monomer	2330.3	370	6.5	
Nonpolar	($^{14}N_2 O)($^{15}N_2 O)$	Heavy monomer	2254.4	290	5.7	
Polar	($^{14}N_2 O)_2$	Sym combo	2326.1	617	2.3	2.696
Polar	($^{14}N_2 O)_2$	Antisym combo	2323.5	109	−0.3	0.119[b]
Polar	($^{15}N_2 O)_2$	Sym combo	2251.1	574	2.4	2.707
Polar	($^{15}N_2 O)_2$	Antisym combo	2248.2	117	−0.5	0.011[b]
Polar	($^{15}N_2 O)($^{14}N_2 O)$ [c]	Light monomer	2323.9	360	0.1	
Polar	($^{15}N_2 O)($^{14}N_2 O)$ [c]	Heavy monomer	2250.7	348	2.0	
Polar	($^{14}N_2 O)($^{15}N_2 O)$ [d]	Light monomer	2325.8	383	2.0	
Polar	($^{14}N_2 O)($^{15}N_2 O)$ [d]	Heavy monomer	2248.6	326	−0.1	
T-shape	($^{14}N_2 O)_2$	Cap monomer	2326.0	500	2.2	
T-shape	($^{14}N_2 O)_2$	Stem monomer	2329.0	282	5.2	
T-shape	($^{15}N_2 O)_2$	Cap monomer	2250.7	473	2.0	
T-shape	($^{15}N_2 O)_2$	Stem monomer	2253.8	272	5.1	

[a]Reference 24, except as indicated.
[b]This work.
[c]The "heavy-inside isomer:" $^{15}N-^{15}N-O$ is monomer B in the polar $[x=90°]$ structure of Fig. 1.
[d]The "light-inside isomer:" $^{14}N-^{14}N-O$ is monomer B in the polar $[x=90°]$ structure of Fig. 1.

Both a- and b-type rotational transitions were observed, but with a-type predominating, which is the opposite of band I where b-type transitions were observed to be stronger. We fixed the ground state parameters to those from the microwave study of polar N_2O dimer.[10] About 102 transitions were assigned, as listed in Table A-I of Ref. 26. The quality of the fit was very good, with a root-mean-square error of 0.0002 cm^{-1}, and the molecular parameters resulting from the analysis are given in the first column of the Table VIII. We also observed the analogous spectrum for band II of the fully ^{15}N-substituted polar N_2O dimer and assigned a total of 112 transitions as listed in Table A-II of Ref. 26. The fit was of similar quality to the normal isotope and the resulting parameters are listed in column 2 of Table VIII.

TABLE VII. Computed CCSD/aug-cc-pVDZ frequency shifts ($\Delta\nu = \nu_{\text{dimer}} - \nu_{\text{monomer}}$) and intensities for N_2O dimers in the region of the monomer ν_3 mode.

Isomer	Isotopomer	Dimer mode	Freq (cm^{-1})	Intensity (km/mol)	Shift (cm^{-1})	Obs shift (cm^{-1}) [a]
Nonpolar	($^{14}N_2 O)_2$	Sym combo	1301.7	0	−5.1	
Nonpolar	($^{14}N_2 O)_2$	Antisym combo	1298.6	188	−8.2	−5.192
Nonpolar	($^{15}N_2 O)_2$	Sym combo	1284.0	0	−5.0	
Nonpolar	($^{15}N_2 O)_2$	Antisym combo	1281.0	179	−8.0	
Nonpolar	($^{14}N_2 O)($^{15}N_2 O)$	Light monomer	1300.3	78	−6.6	
Nonpolar	($^{14}N_2 O)($^{15}N_2 O)$	Heavy monomer	1282.4	105	−6.6	
Polar	($^{14}N_2 O)_2$	Sym combo	1314.1	85	7.2	5.309
Polar	($^{14}N_2 O)_2$	Antisym combo	1299.5	82	−7.4	
Polar	($^{15}N_2 O)_2$	Sym combo	1296.0	81	7.0	
Polar	($^{15}N_2 O)_2$	Antisym combo	1281.8	78	−7.2	
Polar	($^{15}N_2 O)($^{14}N_2 O)$ [b]	Light monomer	1299.8	133	−7.0	
Polar	($^{15}N_2 O)($^{14}N_2 O)$ [b]	Heavy monomer	1295.7	31	6.6	
Polar	($^{14}N_2 O)($^{15}N_2 O)$ [c]	Light monomer	1314.0	79	7.2	
Polar	($^{14}N_2 O)($^{15}N_2 O)$ [c]	Heavy monomer	1281.8	85	−7.2	
T-shape	($^{14}N_2 O)_2$	Cap monomer	1305.5	93	−1.4	
T-shape	($^{14}N_2 O)_2$	Stem monomer	1312.3	91	5.4	
T-shape	($^{15}N_2 O)_2$	Cap monomer	1287.7	89	−1.3	
T-shape	($^{15}N_2 O)_2$	Stem monomer	1294.3	86	5.2	

[a]Reference 9.
[b]the "heavy-inside isomer:" $^{15}N-^{15}N-O$ is monomer B in the polar $[x=90°]$ structure of Fig. 1.
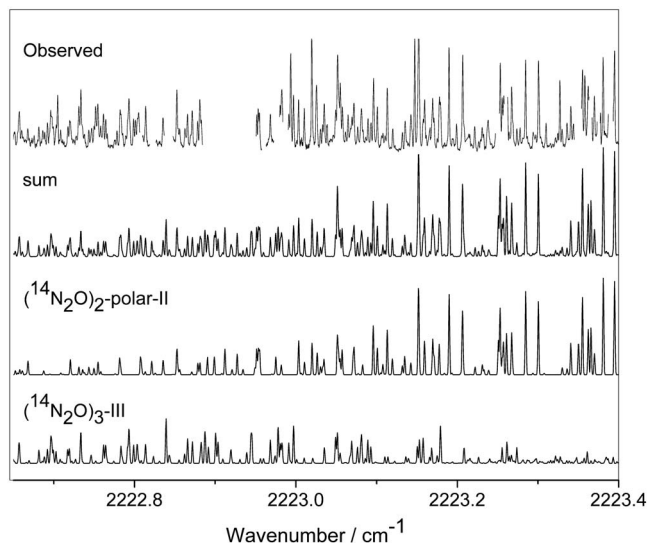[c]the "light-inside isomer:" $^{14}N-^{14}N-O$ is monomer B in the polar $[x=90°]$ structure of Fig. 1.

FIG. 5. Part of "band II" of polar $(N_2O)_2$ in the region of the monomer ν_1 vibration. The top trace is the observed spectrum, with a gap in a region of strong N_2O monomer absorption. The three lower traces are simulations. In this spectral region, there is some weaker structure due to a known (Ref. 24) band of the $^{14}N_2O$ trimer (simulated in the bottom trace), together with the dominant structure of interest here due to band II of polar $(N_2O)_2$ (simulated in the second trace from the bottom). The sum of these two simulations (second trace from top) provides a very good match with experiment.

IV. DISCUSSION AND CONCLUSIONS

Examining the changes in rotational parameters between the ground and excited states for the new band II of the polar isomer reveals that there is substantial decrease in A ($\approx 0.9\%$), accompanied by smaller increases in B ($\approx 0.3\%$) and C ($\approx 0.15\%$). In the case of band I, all three rotational parameters were observed to decrease upon excitation.[11] Though the effect is small, the implication of the increases in B and C for band II is that the intermolecular separation is

TABLE VIII. Molecular parameters for band II of the polar N_2O dimer (in cm^{-1}).[a]

	$(^{14}N^{14}N^{16}O)_2$	$(^{15}N^{15}N^{16}O)_2$
ν_0	2223.8749(1)	2154.7370(1)
A'	0.306 407(32)	0.295 543(28)
B'	0.054 288 4(48)	0.051 947 8(54)
C'	0.045 97 90(32)	0.044 054 7(46)
$10^5 \times \Delta_{K'}$	1.33(18)	1.06(20)
$10^6 \times \Delta_{JK'}$	$-2.55(44)$	$-2.54(37)$
$10^6 \times \Delta_{J'}$	0.300(25)	0.274(27)
$10^6 \times \delta_{K'}$	0.6338[b]	0.6338[b]
$10^7 \times \delta_{J'}$	0.57(21)	0.51(26)
A''	0.309 171 3[b]	0.298 119 0[b]
B''	0.054 124 0[b]	0.051 805 6[b]
C''	0.045 919 2[b]	0.044 004 0[b]
$10^5 \times \Delta_{K''}$	1.267[b]	1.267[b]
$10^6 \times \Delta_{JK''}$	-2.7359[b]	-2.7359[b]
$10^6 \times \Delta_{J''}$	0.3037[b]	0.3037[b]
$10^6 \times \delta_{K''}$	0.6338[b]	0.6338[b]
$10^7 \times \delta_{J''}$	0.5945[b]	0.5945[b]

[a]Uncertainties in parentheses are 1σ from the least-squares fits in units of the last quoted digit.
[b]Ground state parameters (and excited state $\delta_{K'}$) were fixed to those from Ref. 10.

TABLE IX. Vibrational shifts and rotational intensity ratios for the two bands of the polar N_2O dimer in the region of the ν_1 band of the N_2O monomer (in cm^{-1}).

	Observed shift (cm^{-1})	Predicted shift (cm^{-1})	Observed intensity ratio (a-type/b-type) [a]
$(^{14}N^{14}N^{16}O)_2$-I	+2.696	+2.3	0.7
$(^{15}N^{15}N^{16}O)_2$-I	+2.707	+2.4	0.7
$(^{14}N^{14}N^{16}O)_2$-II	+0.119	-0.3	1.8
$(^{15}N^{15}N^{16}O)_2$-II	+0.011	-0.5	1.8

[a]Note that the dipole transition moment ratios are the square roots of these values.

slightly reduced in this excited vibrational state. We note that this trend is consistent with the fact that band II is redshifted relative to band I since the redshift implies (slightly) stronger binding in the excited state.

Table IX compares the observed and theoretical vibrational shifts for bands I and II of both polar N_2O dimer isotopomers, repeated from Table VI for emphasis. The agreement is very good, although the *ab initio* predictions are uniformly slightly "redder" than is observed. Indeed, the predicted frequency *differences* between bands I and II are almost perfect. We also give in Table IX the observed relative intensities of the a- and b-type transitions in bands I and II, which were similar for both isotopomers. The fact that b-type transitions are stronger for band I and a-type transitions for band II seems consistent with the known structure of the polar N_2O dimer. As shown, for example, in Fig. 3 of Ref. 10, the average projection of the N_2O monomer axes on the b inertial axis of the dimer is about 1.3 times greater than on the a-axis, so b-type transitions predominate when the monomers vibrate in-phase. When they vibrate out-of-phase, both the a- and b-type moments tend to cancel, but the former are less affected since the inequivalence of the two monomers is likely to be more significant in the a-axis direction.

For the nonpolar isomer, the agreement between theory and experiment for the vibrational shifts is not as good as for the polar, with the sign calculated correctly but the magnitude overestimated in both the ν_1 and ν_3 monomer regions (Tables V and VI). This of course refers to the allowed antisymmetric dimer mode, since there are no experimental values for the forbidden symmetric mode. It is reasonable to conjecture that the calculated differences between the antisymmetric and symmetric modes may be more reliable than their absolute values, as we noted for the polar isomer. If this is true, then the best estimates for the vibrational shifts for the symmetric modes of the nonpolar $^{14}N_2O$ dimer would be -1.7 and -2.1 cm^{-1} in the ν_1 and ν_3 monomer regions, respectively.

The only experimental information on the intermolecular frequencies of the N_2O dimer comes from the observation of a combination band at 2249 cm^{-1} in the ν_1 monomer region involving the torsional (out-of-plane) vibration.[12] However in order to obtain a torsional frequency from this band, it is necessary to know the frequency of the (forbidden) symmetric fundamental (N–N stretch) mode for the nonpolar dimer. If we use the new "best estimate" discussed in the previous

paragraph (-1.7 cm^{-1}), then the combination band implies a torsional frequency of 27.3 cm^{-1}, as compared to our previous[12] value of 21.5 cm^{-1}, which was based on an older theoretical estimate[23] for the forbidden symmetric mode. We note that this new value is in rather good agreement with the present theoretical value of 30 cm^{-1} (Table V). Perfect agreement cannot be expected here, because the theoretical value is a harmonic one (anharmonic effects may be relatively large in a weakly bound complex), and because the experimental value refers to the torsional frequency when the ν_1 monomer vibration is excited, which may not be identical to that in the ground state.

In conclusion, we performed *ab initio* calculations on the N_2O-N_2O PES at various levels of theory in order to shed some light on recent spectroscopic observations and to guide future experiments. Our best prediction for the binding energy (D_e) of the most stable nonpolar isomer is 598 cm^{-1}, but this value still has a rather substantial uncertainty of about 200 cm^{-1}. Compared to results at the MP2 and PW91 levels, we find that CCSD results reduce the errors in rotational constants from over 10% to less than 3% in the case of the polar N_2O isomer. Although the T-shaped N-in isomer is relatively stable, it is not likely to be experimentally observable since there is at most only a low barrier for its conversion to the (observed) slipped-parallel polar isomer. Theoretical predictions of infrared vibrational frequencies and frequency shifts upon dimerization can be extremely useful in the experimental location of these bands. This has been demonstrated in the present paper by our identification of the previously overlooked and relatively weak out-of-phase version ("band II") of the NNO stretch of the polar N_2O dimer, which accompanies the ν_1 monomer band.

ACKNOWLEDGMENTS

[1] J. Sadlej and M. Sicinski, J. Mol. Struct.: THEOCHEM **204**, 1 (1990).
[2] K. Mogi, T. Komine, and K. Hirao, J. Chem. Phys. **95**, 8999 (1991).
[3] L. M. Nxumalo, T. A. Ford, and A. J. Cox, J. Mol. Struct.: THEOCHEM **307**, 153 (1994).
[4] H. Valdés and J. A. Sordo, J. Phys. Chem. A **108**, 2062 (2004).
[5] Z. S. Huang and R. E. Miller, J. Chem. Phys. **89**, 5408 (1988).
[6] H.-B. Qian, W. A. Herrebout, and B. J. Howard, Mol. Phys. **91**, 689 (1997).
[7] Y. Ohshima, Y. Matsumoto, M. Takami, and K. Kuchitsu, Chem. Phys. Lett. **152**, 294 (1988).
[8] M. Dehghani, M. Afshari, Z. Abusara, N. Moazzen-Ahmadi, and A. R. W. McKellar, J. Chem. Phys. **126**, 164310 (2007).
[9] M. Dehghany, M. Afshari, R. I. Thompson, N. Moazzen-Ahmadi, and A. R. W. McKellar, J. Mol. Spectrosc. **252**, 1 (2008).
[10] N. R. Walker, A. J. Minei, S. E. Novick, and A. C. Legon, J. Mol. Spectrosc. **251**, 153 (2008).
[11] M. Dehghany, M. Afshari, Z. Abusara, C. Van Eck, and N. Moazzen-Ahmadi, J. Mol. Spectrosc. **247**, 123 (2008).
[12] M. Dehghany, M. Afshari, N. Moazzen-Ahmadi, and A. R. W. McKellar, Phys. Chem. Chem. Phys. **10**, 1658 (2008).
[13] S. Tsuzuki, T. Uchimaru, K. Sugawara, and M. Mikami, J. Chem. Phys. **117**, 11216 (2002).
[14] Y. Ohshima, Y. Matsumoto, M. Takami, and K. Kuchitsu, Chem. Phys. Lett. **147**, 1 (1988).
[15] M. J. Frisch, G. W. Trucks, H. B. Schlegel, *et al.*, GAUSSIAN 03, revision C.02, Gaussian, Inc., Wallingford, CT, 2004.
[16] J. P. Perdew, in *Electronic Structure of Solids '91*, edited by P. Ziesche and H. Eschrig (Akademie Verlag, Berlin, 1991), p. 91.
[17] C. Møller and M. S. Plesset, Phys. Rev. **46**, 618 (1934).
[18] J. Cizek, Adv. Chem. Phys. **14**, 35 (1969).
[19] R. J. Bartlett, J. Phys. Chem. **93**, 1697 (1989).
[20] G. E. Scuseria and H. F. Schaefer III, J. Chem. Phys. **90**, 3700 (1989).
[21] T. H. Dunning, Jr., J. Chem. Phys. **90**, 1007 (1989).
[22] D. E. Woon and T. H. Dunning, Jr., J. Chem. Phys. **103**, 4572 (1995).
[23] C. Dutton, A. Sazonov, and R. A. Beaudet, J. Phys. Chem. **100**, 17772 (1996).
[24] M. Dehghany, M. Afshari, N. Moazzen-Ahmadi, and A. R. W. McKellar, J. Chem. Phys. **130**, 044303 (2009).
[25] PGOPHER, a program for simulating rotational structure, C. M. Western, University of Bristol, UK, http://pgopher.chm.bris.ac.uk.
[26] See AIP Document No E-JCPSA6-130-010917 for a listing of line positions and rotational assignments for band II of the polar isomer of N_2O dimer. For more information on EPAPS, see http://www.aip.org/epaps/epaps.html.